ACS OMEGA

http://pubs.acs.org/journal/acsodf

Article

Investigation of the Microscopic Process of the Media Coalescence Treatment of Water-in-Oil Emulsion

Min Meng and Qiang Yang*

Cite This: *ACS Omega* 2023, 8, 11908−11915

Read Online

ACCESS | Metrics & More | Article Recommendations | Supporting Information

ABSTRACT: Medium coalescence technology is a research hotspot for the separation of oil-in-water emulsions. However, the coalescence mechanism is still unclear, making it challenging to effectively improve the separation performance. Herein, the microscopic mechanism of medium coalescence was revealed. We found that the effective collision positions under the action of the flow field include the exposed granule surface, adherent droplet surface, and three-phase contact line. Furthermore, a numerical model of the microscopic process of water-in-oil emulsion permeation through a granular bed was established. The effects of different parameters (including the number of medium layers, Reynolds number, and inlet concentration) on the microscopic process of capturing dispersed-phase droplets in the bed and the pressure drop in the coalescence area were studied. The numerical results show that the droplets form the bridging structure between the granules. On the one hand, the bridging structure promotes the capture of the droplets by the bed; on the other hand, it causes pressure-drop fluctuations in the coalescence area and asymmetric distribution of the velocity field.

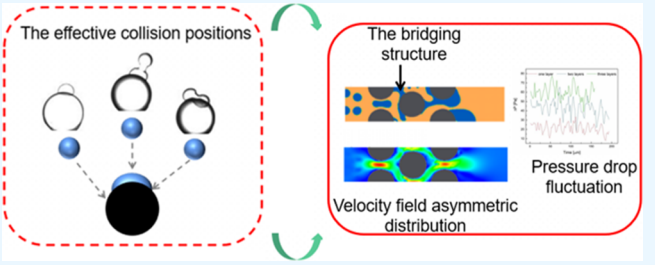

1. INTRODUCTION

Water-in-oil (W/O) emulsions are ubiquitous in oil exploitation and processing.[1−5] Water in oil causes serious harm, such as a reduction in the viscosity of lubricating oil, resulting in lubrication shortage; moreover, it causes equipment metal parts to rust, seriously shortening the service life of the equipment.[6−8] Therefore, it is necessary to remove the water present in the oil. However, water-in-oil emulsion usually has strong interface stability characteristics, causing dehydration problems.[9,10] Commonly used oil dehydration methods include gravity sedimentation, chemical demulsification, vacuum dehydration, centrifugal separation, and electric field dehydration.[2,11−14] However, these methods have many disadvantages, such as high energy consumption (electric field and vacuum dehydration), secondary pollution (chemical demulsification), and low efficiency (centrifugal separation and gravity sedimentation).[15−17] In recent years, media coalescence technology has attracted wide attention from domestic and foreign scholars owing to its advantages of high efficiency, being environmentally friendly, and low energy consumption.[18]

Coalescence is the process through which multiple tiny dispersed-phase droplets collide with each other and fuse into a larger droplet. At the macroscopic level, the coalescence separation mechanism takes advantage of the difference between the affinities of the oil and water phases toward the coalescing material, causing the dispersed-phase droplets to grow from small to large on the coalescing medium and then to be removed from the continuous phase. Hazlet studied the variation of water droplets in coalescing materials. They found that the following three main processes were involved in the coalescence and separation of droplets: approach and collision, drainage and adhesion, and droplet release.[19] Researchers generally agree that bed characteristics, emulsion properties, and operating conditions considerably affect coalescence.[20,21] Many researchers believe that the longer the bed length, the longer the residence time of the emulsion in the bed, which is beneficial to improve the separation efficiency. However, Li believes that there is a critical value of the bed length beyond which the bed separation efficiency no longer increases.[22,23] Generally, superficial flow velocity is a crucial factor in determining the coalescence efficiency, and an increase in superficial velocity decreases the separation efficiency.[24,25] Šećerov Sokolović experimentally and mathematically reasoned to obtain critical velocity under different operating conditions and determined that the separation efficiency was slightly affected by the superficial flow velocity when the superficial flow velocity was lower than the critical flow rate.[26] Moreover, Li concluded that the coalescence efficiency decreases with increasing inlet concentration; however, Zhou and Maiti had the opposite opinion. Generally, the smaller the characteristic

Received: November 12, 2022
Accepted: February 13, 2023
Published: March 22, 2023

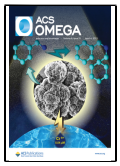

https://doi.org/10.1021/acsomega.2c07274
ACS Omega 2023, 8, 11908−11915

size of the coalescence materials, the better the separation performance.[22−24] Magiera and Blass explored the coalescence effect of three fiber diameters on droplets of different sizes. They found that the coalescence efficiency of droplets increased remarkably with decreasing fiber diameter.[27] Kulkarni et al. designed layered fiber filters and examined the effect of the ratio of hydrophobic and hydrophilic fibers on the separation effect.[7] They also studied the separation effect of a composite bed of a coalescence material made using nano- and micron-scale fibers. They found that adding nanofibers to the coalescence bed resulted in a pronounced increase in the bed pressure drop.[28] The processes occurring in coalescence beds are very complex, and the separation mechanism has been unclear until now. However, researchers have focused on macroscopic separation performance and rarely reported the study of the coalescence mechanism, especially the microscopic process of droplets passing through the coalescence bed in the liquid-phase environment.[29] The absence of research on the microscopic mechanism of coalescence separation has seriously restricted the further development and application of coalescers.

We aim to study the microscopic process of water-in-oil emulsion passing through the coalescence bed in more detail and reveal the microscopic mechanism of coalescence separation. Moreover, an experimental platform for the granule-droplet coalescence microscopic process under the action of the flow field is built, the microscopic process of water-droplet coalescence on granules is observed, and the location of the effective collision is investigated. Furthermore, the microscopic process of water-in-oil emulsion permeation through the coalescence bed was analyzed, and the effects of the number of medium layers, Reynolds number *Re*, and inlet concentration on the coalescence process of dispersed-phase droplets and pressure drop in the coalescence region were considered.

2. EXPERIMENTAL SECTION

2.1. Experimental Materials and Instruments. *n*-Octane (density is 703 kg·m^{-3}, viscosity is 0.547 mPa·s, surface tension is 28.5 mN·m^{-1}), deionized water (density is 998.5 kg·m^{-3}, viscosity is 2.476 mPa·s, surface tension is 73.6 mN·m^{-1}), and glass beads (surface energy is 57.8 dnyes·cm^{-1}) were purchased from Shanghai Maclean Biochemical Technology Co., Ltd. (China), Aladdin Reagent Co., Ltd. (Shanghai), and Tianjin Ibiza Glass Bead Co., Ltd. (China), respectively.

The capillary glass tube and organic glass cylinder (30 mm × 30 mm × 30 mm) were made in-house. The microinjection pump (LongerPump, MF-401), infusion pump (Sino, LD-P2020), high-speed camera (NAC, ACS-1M60, maximum frame rate of 100,000 fps), and contact angle instrument (Kino, SL200KB) were used.

2.2. Experimental Process. Figure 1 shows the experimental device of the effective collision location under the action of the flow field, which is divided into three parts: droplet generation, fluid delivery, and video recording systems. The microinjection pump pushes *n*-octane out of the capillary glass tube. When the gravity of the droplet is enough to overcome the surface tension, the formed *n*-octane droplet drips down from the head of the capillary glass tube. The velocity of fluid movement is regulated by adjusting the flow rate of the infusion pump. The collision behavior of the water droplets under the action of the flow field is recorded using a high-speed camera with a shooting speed of 10,000 fps using luminescence to adjust the brightness of the shooting environment.

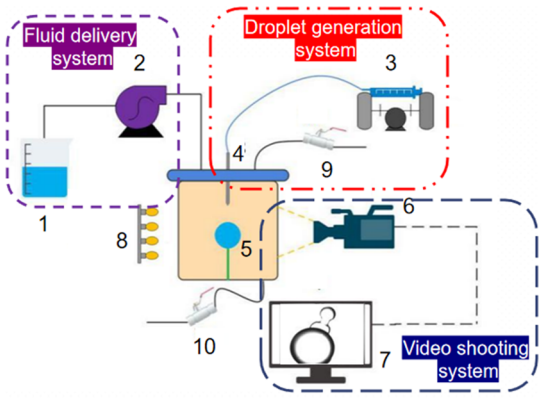

Figure 1. Experimental device of the effective collision location under the action of the flow field.

During the experiment, the glass granule was fixed in the appropriate position in the organic glass cylinder. Additionally, we added an appropriately large amount of *n*-octane to the beaker, opened the exhaust valve, and closed valve V. The infusion pump flow rate was adjusted so that *n*-octane flows into the organic glass cylinder at a specific constant flow rate. Next, we switched on the white luminescence LED lamp, adjusted the location of the high-speed camera and the organic glass cylinder through the elevator, and adjusted the magnification and focal length of the camera using a computer software to obtain a clear image. The injection volume of the microinjection pump was adjusted to make the capillary glass tube extrude droplets of the right size, and a high-speed camera captured the dynamic behavior of the droplets colliding with the granule.

3. SIMULATION SECTION

3.1. Model Description. Based on the effective collision location study, we continue to analyze the microscopic process of water-in-oil emulsion permeation through the coalescence bed using numerical simulations. Figure 2 shows the computational domain of this process. The model is simplified as a two-dimensional model to reduce the computational cost. The calculation domain with a size of 240 × 32 μm^2 is divided into three regions: the feed side, coalescence region, and permeation side. Additionally, dispersed-phase water droplets with 8 μm diameters are randomly distributed on the feed side, and the water-in-oil emulsion passes through the granular bed with a certain velocity.

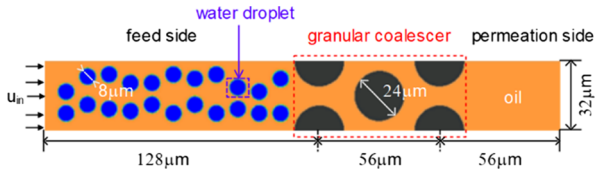

Figure 2. Computational domain of the microscopic process of water-in-oil emulsion permeation through the coalescence bed.

https://doi.org/10.1021/acsomega.2c07274
ACS Omega 2023, 8, 11908−11915

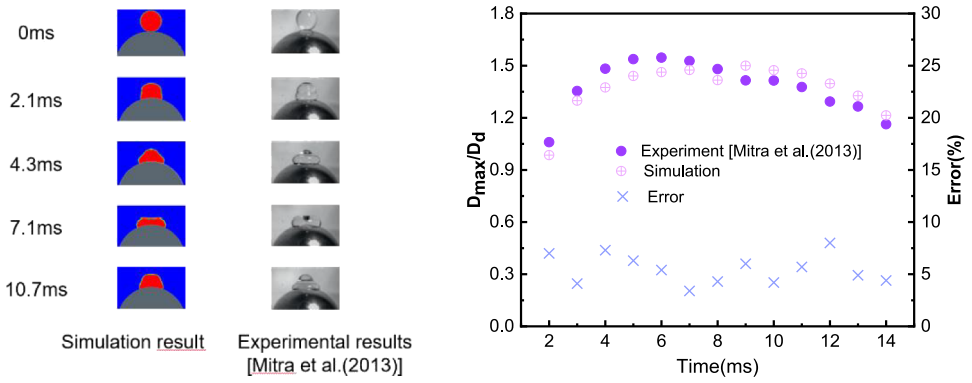

(a) (b)

Figure 3. Comparison of simulation results with experimental results: (a) qualitative analysis; (b) quantitative analysis.

Oil is the continuous phase in the channel, and its dynamic viscosity and density are 2.3 mPa·s and 730 kg·m^{-3}, respectively. The dispersed phase is water droplets; its dynamic viscosity and density are 1 mPa·s and 980 kg·m^{-3}, respectively. The interfacial tension of water in oil is 36 mN·m^{-1}.

3.2. Governing Equations. This study used the coupled level set and volume-of-fluid (CLSVOF) method to track the phase interface. The method uses the level-set function to calculate the volume fraction of the VOF. Simultaneously, it corrects the level-set function using the volume fraction of the VOF.[30] Therefore, this technique overcomes the drawbacks of the level set, and VOF methods can accurately calculate the curvature and normal direction of the phase interface and perform a more accurate capture of the phase interface. The governing equation of the microscopic process of water-in-oil emulsion permeation through the coalescence bed includes the continuity and momentum equations. The Eulerian forms of these two equations are given below.

Continuity equation:

$$\nabla g\vec{v} = 0 \tag{1}$$

Momentum equation:

$$\frac{\partial(\rho\vec{v})}{\partial t} + \nabla\cdot(\rho\vec{v}\vec{v}) = -\nabla P + \nabla\cdot[\mu(\nabla\vec{v} + (\nabla\vec{v})^{\mathrm{T}})] + \rho\vec{g} + \vec{F} \tag{2}$$

Here, ρ and μ are the mixing density and viscosity of oil and water phases, respectively, $\vec{v}$ is the velocity of the fluid, P is the pressure, $\vec{g}$ is the acceleration due to gravity, and $\vec{F}$ is the volume surface tension term.

The physical properties in the equations are determined by weighing the volume fraction of physical properties within each control body. For a two-phase system, the density and viscosity in each control body are as follows.

$$\rho = \phi_w\rho_w + (1 - \phi_w)\rho_o \tag{3}$$

$$\mu = \phi_w\mu_w + (1 - \phi_w)\mu_o \tag{4}$$

The VOF method implements phase interface tracing by defining a volume function $F(\Omega, t)$ (Ω is the computational grid cell), with $F(\Omega, t)$ representing the volume fraction occupied by the fluid in the grid cell, i.e.,

$$\begin{aligned} &F(\Omega, t) = 1, \ \text{only the oil phase in } \Omega \\ &F(\Omega, t) = 0, \ \text{only the water phase in } \Omega \end{aligned} \tag{5}$$

$0 < F(\Omega, t) < 1$, Ω across the interface between oil and water phases.

The level-set method implements phase interface tracking by defining a symbolic distance function $\phi(x)$, i.e.,

$$\phi(x)\begin{cases} >0 & x \text{ is located in the water phase} \\ =0 & x \text{ is located in the interface between oil and water} \\ <0 & x \text{ is located in the oil phase} \end{cases} \tag{6}$$

The curvature k of the kinematic interface and its normal vector $\vec{n}$ are defined subsequently.

$$k = \nabla\cdot\frac{\nabla\phi}{|\nabla\phi|} \tag{7}$$

$$\vec{n} = \frac{\nabla\phi}{|\nabla\phi|} \tag{8}$$

The Heaviside function is introduced to smooth the viscosity and density at the phase interface to avoid numerical instability near the phase interface due to the significant difference in viscosity and density between the two phases.

$$H(\phi) = \begin{cases} 0, & \phi < -l \\ \frac{1}{2}\left[1 + \frac{\phi}{l} - \frac{1}{\pi}\sin\left(\frac{\pi\phi}{l}\right)\right], & -l < \phi < l \\ 1, & \phi > l \end{cases} \tag{9}$$

The surface tension σ using the continuum surface force model is described as follows:[31]

$$F_\sigma = \sigma k\zeta(\phi)\frac{\partial\phi}{\partial x_i} \tag{10}$$

$$\zeta(\phi) = \frac{\mathrm{d}H(\phi)}{\mathrm{d}\phi} \tag{11}$$

CLSVOF uses segmented lines instead of curves for the construction of the phase interface, where the distance function ϕ is used to calculate the acquisition of the normal

https://doi.org/10.1021/acsomega.2c07274
ACS Omega 2023, 8, 11908−11915

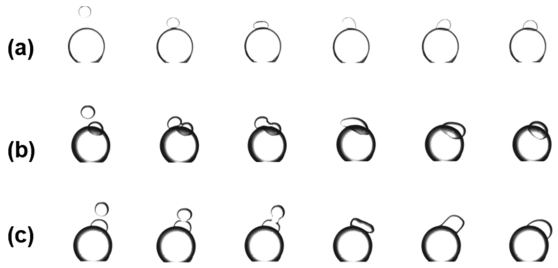

(a)The surface of exposed granules ; (b)the three-phase contact line ; (c)the surface of adhered droplets.

(Experimental conditions : Droplet diameter _3.5mm , Granule diameter_10mm,We_0.0285)

Figure 4. Collision behavior. (a) Surface of exposed granules; (b) three-phase contact line; (c) surface of adhered droplets (experimental conditions: droplet diameter_3.5 mm, granule diameter_10 mm, *We*_0.0285).

vector of the phase interface, and, using the following equation to reinitialize, the geometric method is used to reinitialize ϕ, i.e., to obtain the minimum distance d from the grid centroid to the interface.

$$\phi = \begin{cases} d, & F(\phi, t) < 0.5 \\ 0, & F(\phi, t) = 0.5 \\ -d, & F(\phi, t) > 0.5 \end{cases} \quad (12)$$

3.3. Numerical Methods. In this study, ANSYS Fluent 18.0 (CFD software) was used to simulate the microscopic process of water-in-oil emulsion permeation through the coalescence bed. The inlet boundary is the velocity inlet, outlet boundary is the pressure outlet, upper and lower boundaries are symmetrical, and the media surface is a nonslip wall.

The finite volume method is used to discretize the governing equations. The simple algorithm is used for pressure−velocity coupling; the least squares cell-based method is used to obtain the gradient solution, PRESTO! is used to find the pressure solution, the Geo-Reconstruct technique is used to acquire the volume fraction solution, and the second order upwind method is used for the momentum and level-set function solutions.

The time step $\Delta t = 10^{-7}$ s, and the maximum number of iterations in Δt is 300. The convergence test demonstrates that the calculation results converge within 300 iterations. The physical quantities near the two-phase boundary, requiring a fine mesh, change drastically, and the phase interface region is grid-encrypted using the adaptive mesh refinement technique.

3.4. Model Validation. Mitra et al. experimentally investigated the dynamic processes of droplets after impacting spherical granules.[32] In this study, the numerical model was validated using the same parameters used in the experiment conducted by Mitra et al. Figure 3 presents the comparison of the simulation and experimental results. Based on Figure 3a, it can be found that the simulation results successfully show the morphological changes after the droplets impact the granules. Based on Figure 3a, it can be observed that the error between the simulated $\frac{D_{max}}{D_d}$ results (where D_{max} is the maximum spreading diameter of the droplet and D_d is the droplet diameter) and the experimental results are within 8%, and the simulation results are consistent with the experimental results. Consequently, it can be concluded that the numerical model of this study has high accuracy and can be used for the simulation study of the microscopic process of water-in-oil emulsion permeation through the coalescence bed.

4. RESULTS AND DISCUSSION

4.1. Effective Collision Location. The effective collision location is where droplets can coalesce into larger droplets or adhere to the coalescence medium after a collision. There are three cases in total where droplets collide with granules—free droplets collide with granule surfaces, free droplets collide with three-phase contact lines, and free droplets collide with the surfaces of adhered droplets—where the three-phase contact lines are the locations where water, oil, and solid phases are in contact with each other. Figure 4 shows the collision behavior of the dispersed phases under the action of the flow field. Based on the figure, it can be observed that when the free droplets contact the surface of the exposed granule, the granule intercepts the free droplets. The droplets gradually spread along the granule surface, where the point of impact is assumed to be the center, and adhere to the surface stably. When the free droplet collides with the three-phase contact line, the free droplet interfacial film breaks instantly, and the free and adhered droplets coalesce at the three-phase contact line. Furthermore, when the free droplet collides with the surface of the adhered droplet, the interfacial film ruptures to form a liquid bridge, and the free and adhered droplets rapidly coalesce. Therefore, the effective collision locations of droplets under the flow field include the surface of exposed granules, the surface of adhered droplets, and the three-phase contact line.

4.2. Effect of Media Layers. Figure 5 shows the permeation of the water-in-oil emulsion through the granular bed under different media layers; it can be seen that the water droplets coalesce and grow up on the feed side near the entrance of the coalescence area. This is due to the water-in-oil emulsion in the flow through the coalescence region near the entrance. Due to the interception of the media, the coalescence region near the entrance produces flow around granules, promoting the collision between the dispersed phase of water-droplet coalescence. When there is one medium layer, the water droplets adhere to the granule surface and coalesce when flowing through the coalescence area. The water droplets form a bridging structure between the granules (Figure 5a1). The bridged water droplets block the flow channel and are immediately forced to slip on the granules' surface (Figure 5a3). The water droplets and the bridging structure coalesce into larger water droplets. The formation of the bridging

https://doi.org/10.1021/acsomega.2c07274
ACS Omega 2023, 8, 11908−11915

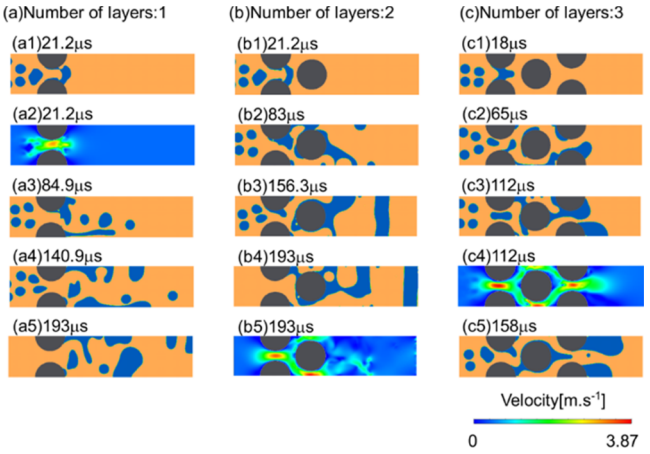

(Simulation conditions：Re_60， inlet concentration_29.8%.)

Figure 5. Microscopic process of trapping and coalescence of dispersed-phase droplets under different media layers (simulation conditions: *Re*_60, inlet concentration_29.8%).

structure enables the granules to capture the water droplets behind them. Due to the small number of medium layers, part of the water droplets escaped from the coalescence area without being captured by the granules (Figure 5a3). When the droplet size increases to a critical value, the grown water droplets fall off the granule surface and move to the permeation side (Figure 5a4,a5).

When the number of medium layers is two, the water droplets adhere to the granules and form a bridging structure (Figure 5b1), and the grown-up water droplets coat the second layer of granules (Figure 5b2). Under normal circumstances, the interfacial tension causes the water droplets to become spherical. However, the dropped water droplets become square (Figure 5b3), possibly due to the smaller size of the geometric model along the *y*-axis. The bridging structure completely blocked the flow channel in the coalescence zone and formed oil-in-water-in-oil droplets (Figure 5b4). At the location of the second layer of granules, the bridging droplets near the upper boundary completely block the flow channel, and the bridging droplets near the lower boundary have not yet completely blocked the flow channel (Figure 5b4). Correspondingly, the fluid flow velocity near the lower boundary is significantly higher than that at the upper boundary (Figure 5b5). Therefore, we can conclude that the bridging structure blocking the flow channel causes the velocity field in the coalescence region to exhibit an asymmetric distribution.

Although the adhered water droplets slip along the granule surface when the number of medium layers is three, the grown water droplets always adhere to the granules in the coalescence area and the grown water droplets do not fall off the granule surface (Figure 5c3,c5). The main reason is that the residence time of water droplets in the coalescence region grows as the number of medium layers increases. Increasing the granular surface area improves the bed's ability to capture water droplets. We again observed an asymmetric velocity field distribution due to the blocking of the flow channel by the bridging structure (Figure 5c3,c4).

The pressure drop is one important economic indicator of coalescence separation technology. The larger the pressure drop, the greater the flow resistance of the fluid flowing through the coalescence bed and the greater the processing cost of coalescence separation technology. Therefore, we studied the effects of layer numbers, Reynolds number, and inlet concentration on pressure drop in the coalescence region. It can be observed from Figure 6 that the larger the number of

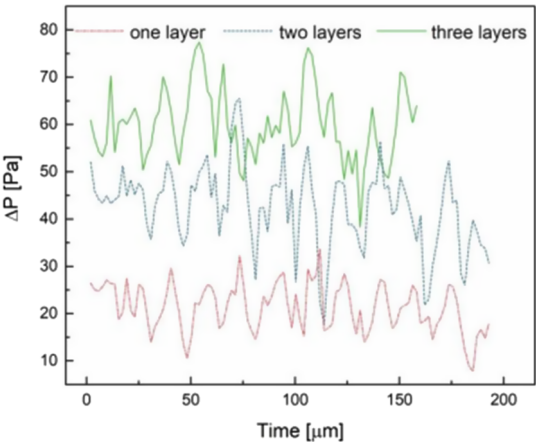

(Simulation conditions: Re_60, inlet concentration_ 29.8 %.)

Figure 6. Pressure drop in the coalescence area under different media layers (simulation conditions: *Re*_60, inlet concentration_29.8%).

media layers, the greater the pressure drop in the coalescence area, and the pressure drop in the coalescence area fluctuates with time. This may be caused by the formation of a bridging structure that blocks the flow channel. When the bridging droplet completely blocks the flow channel, the pressure drop in the coalescence area is the largest. In the case of three medium layers, the bridging structure entirely blocks the flow channel at 112 μs and the pressure drop simultaneously reaches a maximum in the agglomeration region.

4.3. Effect of the Reynolds Number. Figure 7 shows the permeation of the water-in-oil emulsion through the granular bed at different Reynolds numbers. It can be seen from Figure 7 that when *Re* is small, i.e., when *Re* = 20, the size of the bridging structure formed is much larger and the bridging structure tends to completely block the flow channel (Figure

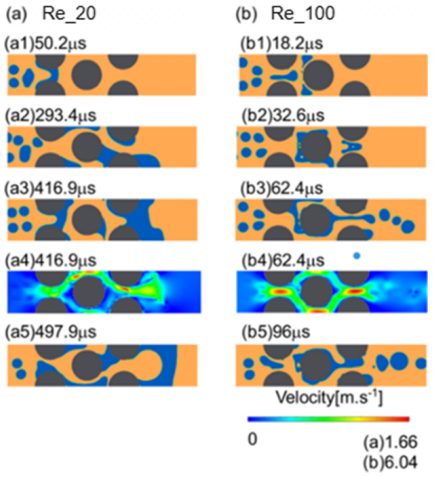

(Simulation conditions: number of media layers: 3, inlet concentration: 29.8 %.)

Figure 7. Microscopic process of trapping and coalescence of dispersed-phase droplets under different Reynolds numbers (simulation conditions: number of media layers: 3, inlet concentration: 29.8%).

https://doi.org/10.1021/acsomega.2c07274
ACS Omega 2023, 8, 11908−11915

7a3). When the inlet velocity is large, i.e., when *Re* = 100, the bridging structure breaks to form a large number of satellite droplets and the satellite droplets quickly flow through the permeation side (Figure 7b3,b5) due to the increase in the Reynolds number, which leads to an increase in the scouring force of the continuous phase fluid acting on the bridging structure. Consequently, the increase in scouring force causes a rise in the amplitude of the interface disturbance of the bridging structure. When the amplitude of the disturbance exceeds the stability conditions of the interface, it causes the droplets to break and produce satellite droplets. Figure 8

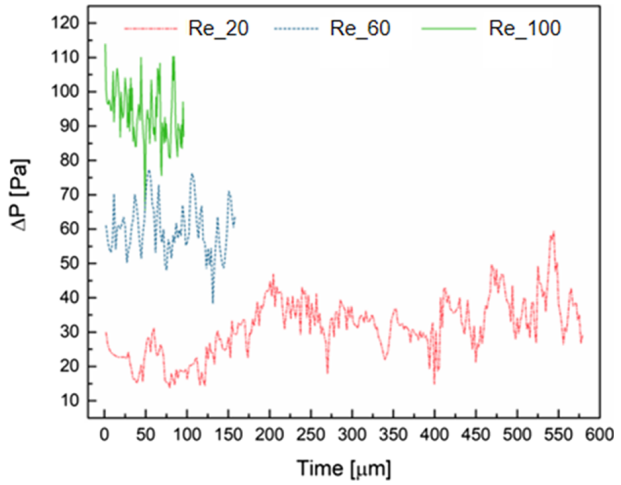

(Simulation conditions: number of media layers: 3, inlet concentration: 29.8 %.)

Figure 8. Pressure drop in the coalescence area at different Reynolds numbers (simulation conditions: number of media layers: 3, inlet concentration: 29.8%).

displays the pressure drop in the coalescence area at different Reynolds numbers. The Reynolds number has a substantial effect on the pressure drop in the coalescence area, and the higher the Reynolds number, the greater the pressure drop in the coalescence area.

4.4. Effect of Inlet Concentration. Figure 9 shows the permeation of the water-in-oil emulsion through the granular bed at different inlet concentrations. It can be seen from Figure 9 that when the inlet concentration is 14.9% (Figure 9a), water droplets adhere to the granule surface; however, no bridging structure is formed between the first layer of the granules (Figure 9a1). The adhered water droplets crawl on the granule surface along the flow direction and move to the downstream side (Figure 9a1,a2). The bridging structure breaks under the scouring action of the fluid to form satellite droplets (Figure 9a3). The bridging structure that completely blocks the flow channel does not form when the inlet concentration is low (14.9%), mainly because the lower the concentration of the dispersed phase, the smaller the number of water droplets per unit volume, which is not conducive to the subsequent coalescence of droplets on the bridging structure. When the inlet concentration is 21.7% (Figure 9b), the droplets tend to form a bridging structure that completely blocks the flow channel because the number of droplets per unit volume increases (Figure 9b4). Figure 10 shows the pressure drop in

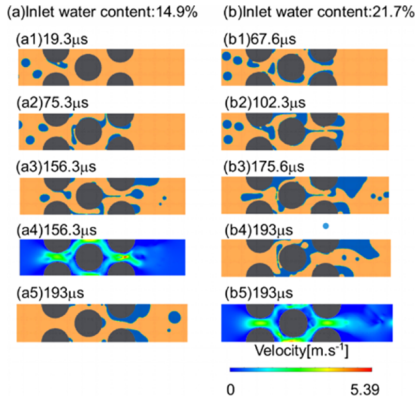

(Simulation conditions: Re_60, number of media layers: 3.)

Figure 9. Microscopic process of trapping and coalescence of dispersed-phase droplets under different inlet concentrations (simulation conditions: *Re*_60, number of media layers: 3).

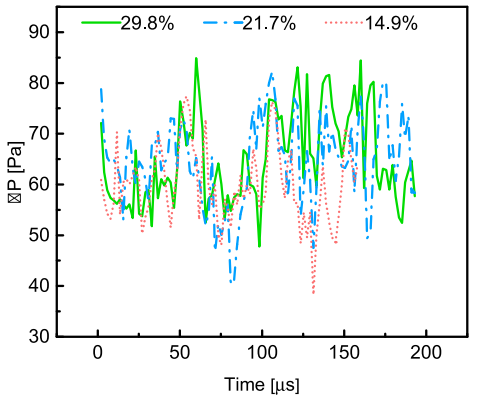

(Simulation conditions: Re_60, number of media layers: 3.)

Figure 10. Pressure drop in the coalescence area at different inlet concentrations (simulation conditions: *Re*_60, number of media layers: 3).

the coalescence area at different inlet concentrations. For more details on the pressure drop, see the supplementary material. It can be seen from Figure 10 that the inlet concentration has no considerable impact on the pressure drop in the coalescence area. However, the greater the inlet concentration, the larger the maximum peak-pressure drop in the coalescence area. For example, when the inlet concentrations are s14.9, 21.7, and 29.8%, the maximum peak-pressure drops in the coalescence area are 77.3, 81.8, and 84.9 Pa, respectively.

5. CONCLUSIONS

We studied the microscopic process of water-in-oil emulsion coalescence separation using experimental and numerical simulation methods. The effective collision locations of liquid droplets under the action of flow fields were analyzed using experimental techniques. The effects of the number of medium layers, Reynolds number, and inlet concentration on droplet demulsification behavior and coalescer pressure drop in the coalescence separation process were investigated using the CLSVOF method. The main conclusions of this study are as follows:

1. Under the action of the flow field, effective collision locations include the exposed granule surface, adhered droplet surface, and three-phase contact line.

https://doi.org/10.1021/acsomega.2c07274
ACS Omega 2023, 8, 11908−11915

2. Although the bridging structure promotes water-droplet capture by the bed, it causes fluctuations in the pressure drop and asymmetric distribution of the velocity field.
3. During the coalescence separation process, the pressure drop fluctuates with time. The higher the number of medium layers and the greater the Reynolds number, the larger the pressure drop. An increase in the inlet concentration increases the maximum peak-pressure drop.

■ ASSOCIATED CONTENT

Supporting Information

The Supporting Information is available free of charge at https://pubs.acs.org/doi/10.1021/acsomega.2c07274.

Effect of inlet concentration on pressure drop in the coalescence area: (a) inlet concentration_29.8%; (b) inlet concentration_21.7%; and (c) inlet concentration_14.9% (PDF)

■ AUTHOR INFORMATION

Corresponding Author

Qiang Yang − *School of Mechanical and Power Engineering, East China University of Science and Technology, Shanghai 200237, P.R. China*; Email: qyang@ecust.edu.cn

Author

Min Meng − *School of Mechanical and Power Engineering, East China University of Science and Technology, Shanghai 200237, P.R. China; Computational Aerodynamics Institute, China Aerodynamics Research & Development Center, Mianyang 621000, P.R. China*; orcid.org/0000-0002-7321-3408

Complete contact information is available at: https://pubs.acs.org/10.1021/acsomega.2c07274

Notes

The authors declare no competing financial interest.

■ ACKNOWLEDGMENTS

This work is supported by the National Natural Science Foundation of China (Grant No. 52000072).

■ REFERENCES

(1) Mohammadian, E.; Taju Ariffin, T. S.; Azdarpour, A.; Hamidi, H.; Yusof, S.; Sabet, M.; Yahya, E. Demulsification of Light Malaysian Crude Oil Emulsions Using an Electric Field Method. *Ind. Eng. Chem. Res.* **2018**, *57*, 13247−13256.

(2) Sousa, A. M.; Pereira, M. J.; Matos, H. A. Oil-in-water and water-in-oil emulsions formation and demulsification. *J. Pet. Sci. Eng.* **2022**, *210*, No. 110041.

(3) Zolfaghari, R.; Fakhru'l-Razi, A.; Abdullah, L. C.; Elnashaie, S. S. E. H.; Pendashteh, A. Demulsification techniques of water-in-oil and oil-in-water emulsions in petroleum industry. *Sep. Purif. Technol.* **2016**, *170*, 377−407.

(4) Souza, A. V.; Mendes, M. T.; Souza, S. T. S.; Palermo, L. C. M.; Oliveira, P. F.; Mansur, C. R. E. Synthesis of Additives Based on Polyethylenimine Modified with Non-ionic Surfactants for Application in Phase Separation of Water-in-Oil Emulsions. *Energy Fuels* **2017**, *31*, 10612−10619.

(5) Gohil, J. M.; Kwon, G.; Bhunia, P.; Dutta, K.; Boukherroub, R. Overview on Oil/Water Separation Techniques and Working Principles. In *Oil−Water Mixtures and Emulsions, Volume 1: Membrane Materials for Separation and Treatment*; ACS Symposium Series, Vol. 1407; American Chemical Society, 2022; pp 247−304.

(6) Eow, J. S.; Ghadiri, M. Electrostatic enhancement of coalescence of water droplets in oil: a review of the technology. *Chem. Eng. J.* **2002**, *85*, 357−368.

(7) Kulkarni, P. S.; Patel, S. U.; Chase, G. G. Layered hydrophilic/hydrophobic fiber media for water-in-oil coalescence. *Sep. Purif. Technol.* **2012**, *85*, 157−164.

(8) Stanfel, C. Fuel filtration: Protecting the diesel engine. *Filtr. Sep.* **2009**, *46*, 22−25.

(9) Kumar, K.; Nikolov, A. D.; Wasan, D. T. Mechanisms of Stabilization of Water-in-Crude Oil Emulsions. *Ind. Eng. Chem. Res.* **2001**, *40*, 3009−3014.

(10) Wang, D.; Yang, D.; Huang, C.; Huang, Y.; Yang, D.; Zhang, H.; Liu, Q.; Tang, T.; Gamal El-Din, M.; Kemppi, T.; et al. Stabilization mechanism and chemical demulsification of water-in-oil and oil-in-water emulsions in petroleum industry: A review. *Fuel* **2021**, *286*, No. 119390.

(11) Panda, S. K.; Buwa, V. V. Effects of Geometry and Internals of a Continuous Gravity Settler on Liquid−Liquid Separation. *Ind. Eng. Chem. Res.* **2017**, *56*, 13929−13944.

(12) Ma, J.; Yao, M.; Yang, Y.; Zhang, X. Comprehensive review on stability and demulsification of unconventional heavy oil-water emulsions. *J. Mol. Liq.* **2022**, *350*, No. 118510.

(13) Akbarian Kakhki, N.; Farsi, M.; Rahimpour, M. R. Effect of current frequency on crude oil dehydration in an industrial electrostatic coalescer. *J. Taiwan Inst. Chem. Eng.* **2016**, *67*, 1−10.

(14) Bahú, J. O.; Miranda, N. T.; Khouri, N. G.; Batistella, C. B.; Cárdenas Concha, V. O.; Maciel, M. R. W.; Schiavon, M. I. R. B.; Maciel Filho, R. Crude oil emulsion breaking: An investigation about gravitational and rheological stability under demulsifiers action. *J. Pet. Sci. Eng.* **2022**, *210*, No. 110089.

(15) Faizullayev, S.; Adilbekova, A.; Kujawski, W.; Mirzaeian, M. Recent demulsification methods of crude oil emulsions − Brief review. *J. Pet. Sci. Eng.* **2022**, *215*, No. 110643.

(16) Wang, D.; Zhao, Z.; Qiao, C.; Yang, W.; Huang, Y.; McKay, P.; Yang, D.; Liu, Q.; Zeng, H. Techniques for treating slop oil in oil and gas industry: A short review. *Fuel* **2020**, *279*, No. 118482.

(17) Ma, F. X.; Hao, B.; Xi, X. Y.; Wang, R.; Ma, P.-C. Aggregation-induced demulsification technology for the separation of highly emulsified oily wastewater produced in the petrochemical industry. *J. Cleaner Prod.* **2022**, *374*, No. 134017.

(18) Hu, D.; Li, L.; Li, Y.; Yang, C. Restructuring the surface of polyurethane resin enforced filter media to separate surfactant stabilized oil-in-water emulsions via coalescence. *Sep. Purif. Technol.* **2017**, *172*, 59−67.

(19) Hazlett, R. N. Fibrous Bed Coalescence of Water. Steps in the Coalescence Process. *Ind. Eng. Chem. Fundam.* **1969**, *8*, 625−632.

(20) Esmaelion, F.; Tavanai, H.; Beigi, A. A. M.; Bazarganipour, M. Application of fibrous structures in separation of water and oil emulsions: A review. *J. Environ. Chem. Eng.* **2022**, *10*, No. 107999.

(21) Bansal, S.; von Arnim, V.; Stegmaier, T.; Planck, H. Effect of fibrous filter properties on the oil-in-water-emulsion separation and filtration performance. *J. Hazard. Mater.* **2011**, *190*, 45−50.

(22) Li, J.; Gu, Y. Coalescence of oil-in-water emulsions in fibrous and granular beds. *Sep. Purif. Technol.* **2005**, *42*, 1−13.

(23) Maiti, S.; Mishra, I. M.; Bhattacharya, S. D.; Joshi, J. K. Removal of oil from oil-in-water emulsion using a packed bed of commercial resin. *Colloids Surf., A* **2011**, *389*, 291−298.

(24) Zhou, Y. B.; Chen, L.; Hu, X. M.; Lu, J. Modified Resin Coalescer for Oil-in-Water Emulsion Treatment: Effect of Operating Conditions on Oil Removal Performance. *Ind. Eng. Chem. Res.* **2009**, *48*, 1660−1664.

(25) Zhou, Y. B.; Tang, X. Y.; Hu, X.-M.; Fritschi, S.; Lu, J. Emulsified oily wastewater treatment using a hybrid-modified resin and activated carbon system. *Sep. Purif. Technol.* **2008**, *63*, 400−406.

(26) Šećerov Sokolović, R. M.; Sokolović, S. M.; Đoković, B. D. Effect of Working Conditions on Bed Coalescence of an Oil-in-Water Emulsion Using a Polyurethane Foam Bed. *Ind. Eng. Chem. Res.* **1997**, *36*, 4949−4953.

(27) Magiera, R.; Blass, E. Separation of liquid-liquid dispersion by flow through fibre beds. *Filtr. Sep.* **1997**, *34*, 369−376.
(28) Kulkarni, P. S.; Patel, S. U.; Patel, S. U.; Chase, G. G. Coalescence filtration performance of blended microglass and electrospun polypropylene fiber filter media. *Sep. Purif. Technol.* **2014**, *124*, 1−8.
(29) Agarwal, S.; von Arnim, V.; Stegmaier, T.; Planck, H.; Agarwal, A. Effect of Fibrous Coalescer Geometry and Operating Conditions on Emulsion Separation. *Ind. Eng. Chem. Res.* **2013**, *52*, 13164−13170.
(30) Guo, Y.; Wei, L.; Liang, G.; Shen, S. Simulation of droplet impact on liquid film with CLSVOF. *Int. Commun. Heat Mass Transfer* **2014**, *53*, 26−33.
(31) Brackbill, J. U.; Kothe, D. B.; Zemach, C. A continuum method for modeling surface tension. *J. Comput. Phys.* **1992**, *100*, 335−354.
(32) Mitra, S.; Sathe, M. J.; Doroodchi, E.; Utikar, R.; Shah, M. K.; Pareek, V.; Joshi, J.; Evans, G. M. Droplet impact dynamics on a spherical particle. *Chem. Eng. Sci.* **2013**, *100*, 105−119.

https://doi.org/10.1021/acsomega.2c07274
ACS Omega 2023, 8, 11908−11915